The Astrophysical Journal Supplement Series, 154:346–351, 2004 September

MODELS FOR THE INFRARED CAVITY OF HH 46/47

A. C. Raga,[1] A. Noriega-Crespo,[2] R. F. González,[1] and P. F. Velázquez[1]
Received 2004 March 23; accepted 2004 May 8

ABSTRACT

We have modeled the limb-brightened cavity seen in the new *Spitzer Space Telescope* IR images of the southwest lobe of HH 46/47 as the bow shock driven by an outflow from a young, low-mass star. We present models in which the outflow is a perfectly collimated, straight jet, models in which the jet precesses, and finally a model in which the outflow takes the form of a latitude-dependent wind. We study cases in which the outflow moves into a constant-density cloud and into a stratified cloud. We find that the best agreement with the observed cavity is obtained for the precessing jet in a stratified cloud. However, the straight jet (traveling in a stratified cloud) also gives cavity shapes close to the observed one. The latitude-dependent wind model that we have computed gives cavity shapes that are substantially wider than the observed cavity. We therefore conclude that the cavity seen in the *Spitzer* observations of the southwest lobe of the HH 46/47 outflow do not seem to imply the presence of a latitude-dependent wind, as it can be modeled successfully with a perfectly collimated jet model.

Subject headings: infrared: ISM — ISM: Herbig-Haro objects — ISM: jets and outflows

1. INTRODUCTION

There are a few molecular outflows from young stars that show limb-brightened "cavities." Objects like L1157 (e.g., Beltrán et al. 2004) show cavities with little or no central emission, while objects like the Orion B molecular jet show cavity-like structures at low radial velocities, which are axially filled at higher radial velocities (Richer et al. 1992). In particular, Lee et al. (2002) have described several objects showing limb-brightened CO emission.

Some Herbig-Haro (HH) jets also show limb-brightened, cavity-like structures that open out from the position of the outflow source. The most striking example to date is probably the L1551 IRS 5 outflow (which contains the HH 454 jet and HH 29). This object shows a large-scale "broken cavity" (with an extent of $\sim 10'$; see Rodríguez et al. 1989) and also a much smaller, limb-brightened structure close to the outflow source (HH 464; see, e.g., Stocke et al. 1988; Mundt et al. 1991), both seen in Hα and in other emission lines. However, it is unclear whether or not the compact, limb-brightened structure is actually a cavity, because both high-resolution optical images (Fridlund & Liseau 1998) and radio continuum interferometric observations (Rodríguez et al. 2003) of the region close to the source indicate that one might actually be seeing a system of two jets (rather than a limb-brightened cavity).

A discussion of (approximately) conical reflection cavities centered on the sources of several HH jets is presented by Reipurth et al. (2000). One of the more remarkable examples of such a "reflection cavity" is that of the northeast lobe of HH 46/47, which has a highly asymmetric structure.

Some HH jets show cavity-like structures that consist of long extensions of the wings of bow shocks. Possibly the first structure of this kind was detected (and identified as such) in HH 34 by Reipurth et al. (1986). One of the more remarkable of such "extended bow shock wing" structures is that observed in H_2 2.12 μm images of the HH 46/47 outflow.

The southwest lobe of this flow is embedded within a Bok globule, only to become visible optically $\sim 2'$ from the source as the faint and compact knot HH 47C (although a central, "knotty jet" structure is seen close to the source at IR wavelengths; see Reipurth & Heathcote 1991). The H_2 2.12 μm map of Eislöffel et al. (1994) shows a series of elongated condensations that appear to trace the extended bow shock wings all the way from knot 47C to $\sim 30''$ from the source.

In a new *Spitzer* IR image of HH 46/47 (see Fig. 1; Noriega-Crespo et al. 2004) the cavity in the southwest lobe is seen in its full glory, and extended bow shock wings are also visible in the northeast lobe (trailing behind the condensation HH 47A). The *Spitzer* image was obtained by co-adding the four Infrared Array Camera (IRAC) channels at 3.6, 4.5, 5.8, and 8 μm, which include in their passbands some of the brightest pure rotational H_2 lines as well as polycyclic aromatic hydrocarbon broad emission features at 6.2 and 6.7 μm.

Figure 1 (Plate 1) is a three-color image of the HH 46/47 outflow that shows a combination of the [S II] 6716+30 (optical) emission with the IRAC 3.6 and 4.5 μm maps. For the first time, the *Spitzer* observations show an HH jet bow shock (HH 47C, which is clearly seen in [S II]) with wings extending toward the source and joining the walls of a conical cavity with its apex at the outflow source. Even though bow-shock wings extending all the way to the source are a general feature of numerical models of HH jets (see, e.g., Downes & Cabrit 2003; Rosen & Smith 2004), the *Spitzer* HH 46/47 map is the first observation of an optically detected HH jet in which such a clear structure of this kind is actually seen at IR wavelengths (although such cavities have previously been observed at radio wavelengths in objects such as the L1157 molecular outflow and the HH 211 molecular jet, see, e.g., Gueth et al. 1998, 1999).

This new result motivates the following questions regarding the production of a bow-shock structure with the shape of the cavity of the southwest lobe of HH 46/47:

[1] Instituto de Ciencias Nucleares, Universidad Nacional Autónoma de México, Apartado Postal 70-543, CP 04510, México DF, Mexico; raga@nuclecu.unam.mx, ricardog@nuclecu.unam.mx, pablo@nuclecu.unam.mx.

[2] *Spitzer* Science Center, California Institute of Technology, MC 314-6, 1200 East California Boulevard, Pasadena, CA 91125; alberto@ipac.caltech.edu.

Can one obtain this with a "standard" (perfectly collimated, nonprecessing) jet model?

Is it necessary to introduce a precession in the ejection?

Is the observed shape evidence for the presence of a less well-collimated, latitude-dependent wind?

Is it necessary to consider a stratification for the surrounding environment?

We illustrate these issues by presenting six gasdynamic models, in which we consider a straight jet, a precessing jet, and a latitude-dependent wind traveling into two environmental configurations. In the first one, we assume that the source is placed within a constant-density cloud and that the outflow eventually emerges into a lower density (and homogeneous) surrounding environment. In the second configuration, we assume that the cloud itself is stratified.

We first discuss the parameters appropriate for the HH 46/47 outflow (§ 2). We then present the shape of the bow-shock cavities for the six resulting outflow/environment configurations described above (§ 3). Finally, we discuss the successes and failures of our models (§ 4).

2. HH 46/47 AND ITS ENVIRONMENT

HH 46/47 is in the Gum Nebula, at a distance of approximately 350 pc from the Sun (see Schwartz 1977). From proper motion and radial velocity measurements (see, e.g., Meaburn & Dyson 1987; Raymond et al. 1994; Eislöffel & Mundt 1994), one obtains an orientation angle of $\approx 35^\circ$ between the outflow axis and the plane of the sky.

With this orientation angle, one obtains deprojected distances of $\approx 5 \times 10^{17}$ cm from the source to knot 47A and of $\approx 7.5 \times 10^{17}$ cm out to knot 47D along the northeast lobe. The single, optically detected knot along the southwest lobe (knot 47C) lies $\approx 7.5 \times 10^{17}$ cm from the source. The full spatial velocities of both lobes of the HH 46/47 outflow have values of ~ 250 km s^{-1} (although both the radial velocities and proper motions vary considerably with position; see Raymond et al. 1994; Eislöffel & Mundt 1994).

In optical images of the outflow, one sees that HH 47C is just emerging beyond the edge of the dark cloud (which hides the outflow source). However, as the southwest lobe is redshifted, it is unclear whether knot 47C actually is physically close to the point at which the jet emerges from the cloud or whether this point lies closer to the source (but is hidden from view by the dark cloud).

In order to model the southwest lobe of HH 46/47, we assume that the outflow source is placed within a dense cloud and that there is an interface between the cloud and a more diffuse medium at a distance of 10^{18} cm from the source. For the diffuse medium, we assume that it has a density $n_{\rm dif} = 10$ cm^{-3} and a temperature $T_{\rm dif} = 1300$ K.

For the dense cloud, we have considered two cases:

1. *Constant-density cloud*.—The cloud has a constant temperature $T_c = 13$ K and number density $n_c = 1000$ cm^{-3}.
2. *Stratified cloud*.—The cloud has a constant temperature $T_c = 13$ K and a stratified density given by

$$n_c = \frac{n_0 r_0^2}{(r + r_0)^2}, \tag{1}$$

where r is the spherical radius (measured from the position of the source) and $n_0 = 10^4$ cm^{-3} and $r_0 = 3.3 \times 10^{17}$ cm are constants. This stratification has a flat density profile close to the source, tends to the singular isothermal sphere solution at large radii (for the appropriate $T_c = 13$ K temperature), and satisfies pressure balance at the interface (at $r_c = 10^{18}$ cm; see above) with the diffuse external medium. In addition, this stratification has a mass of $\sim 10\ M_\odot$ within the radius r_c.

For the jet, we have considered an outflow with a (constant) ejection velocity $v_j = 250$ km s^{-1} and mass-loss rate $\dot{M}_j = 10^{-6}\ M_\odot$ yr^{-1} (these parameters being consistent with those determined for this object by Hartigan et al. 1994). We have then considered the three following possibilities:

M1: straight jet.—An initially perfectly collimated jet ejected in a time-independent direction, with an initial radius $r_j = 2 \times 10^{16}$ cm (which for the mass-loss rate given above implies an initial density $n_j = 940$ cm^{-3}) and temperature $T_j = 1000$ K.

M2: precessing jet.—The same as above, but with an ejection direction that precesses in a cone of half–opening angle $\alpha = 5^\circ$ with a period $\tau = 300$ yr.

M3: latitude-dependent wind.—A spherical wind with a constant ejection velocity but with a latitude-dependent density of the form

$$n_w(\theta) = n_0 \left(\frac{\sin \theta_0}{\sin \theta} \right)^2, \quad \theta > \theta_0,$$

$$n_w(\theta) = n_0, \quad \theta \leq \theta_0, \tag{2}$$

at the spherical radius $r_w = 10^{17}$ cm at which we inject the wind. In this equation, θ is the angle measured from the symmetry axis. We have fixed $\theta_0 = 2^\circ$ and determined $n_0 = 4700$ cm^{-3} in order to have the mass-loss rate of $10^{-6}\ M_\odot$ yr^{-1} given above in one hemisphere of the wind. This latitude-dependent wind configuration is an approximation to the asymptotic solution found by Shu et al. (1995) and Li & Shu (1996) for their "X-wind" magnetocentrifugal wind model. The parameterized latitude-dependent density (eq. [2]) has a pole-to-equator density ratio that depends on the angle θ_0. For our particular choice of θ_0 ($= 2^\circ$, see above), we obtain a density ratio of ~ 800.

We have therefore computed two versions of models M1, M2, and M3, with the constant-density cloud and stratified cloud environments, respectively. Models M1 and M3 were computed with the radiative, two-dimensional (axisymmetric) version of the YGUAZÚ-A code, and model M3 with the three-dimensional version. The code is described in detail by Raga et al. (2000), and the nonequilibrium ionization/cooling network that was used is described by Raga et al. (2002). The gravity force necessary to preserve the stratification of the cloud has been included in the appropriate simulations. In all of the simulations, both the environment and the injected jet material are neutral (except for C and S, which are assumed to be singly ionized). Models M1 and M3 were computed on a five-level, binary adaptive grid with a maximum resolution of 3.9×10^{15} cm (along the three axes), and model M2 on a four-level grid with a maximum resolution of 7.8×10^{15} cm. The obtained results are described in § 3.

3. MODEL RESULTS

Figures 2–4 show the density stratifications at two different integration times obtained from models M1, M2, and

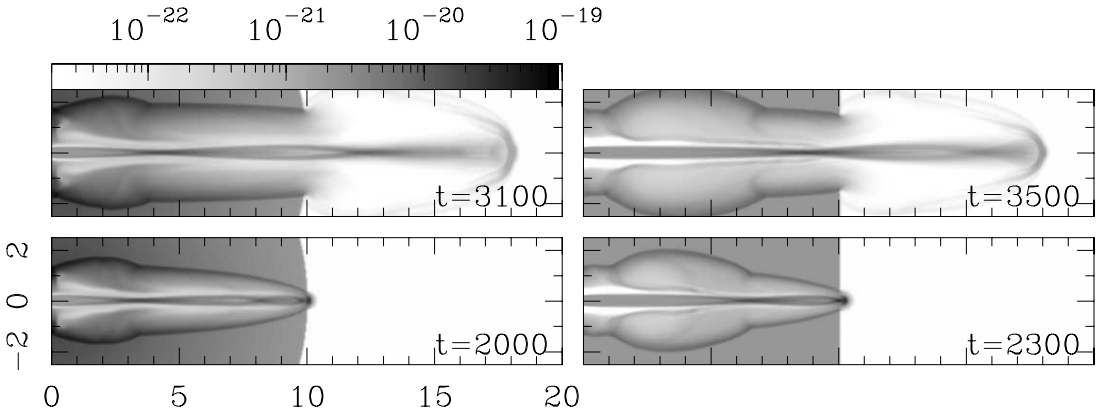

FIG. 2.—Density stratifications obtained for model M1 (straight jet; see §§ 2 and 3) displayed with a logarithmic gray scale (given in g cm^{-3} by the bar on the top left). The distances along (*abscissa*) and perpendicular (*ordinate*) to the outflow axis are labeled in units of 10^{17} cm. The right panels show two time frames (labeled with the integration time, given in years) for the constant-density cloud environment (in which the cloud occupies the left half of the displayed domain and has a plane interface with the diffuse medium on the right half). The left panels show two time frames for the stratified cloud environment in which the cloud has a spherically symmetric density stratification (see eq. [1] of § 2).

M3 with the constant-density cloud and the stratified cloud environments. The results shown correspond to times when the jet is just emerging from the dense cloud (*bottom panels)* and when the head of the jet has reached a distance of $\sim 1.8 \times 10^{18}$ cm from the source (*top panels*).

All of the models have a leading bow shock with wings extending all the way to $z = 0$ (where z is the distance measured along the axis of the outflow). In all cases, there is a dense shell of material right behind the bow-shock wings, so that cavities with dense "walls" are obtained.

For all of the models (Figs. 2–4), the cavities obtained with the stratified cloud environment are narrower than the cavities obtained for the constant-density cloud case. In model M2 (precessing jet), the simulation with the stratified cloud environment has a narrow "waist" around the injection point, while the constant-density cloud model shows bow-shock wings that open out all the way from the head of the jet to $z = 0$. On the other hand, model M1 (straight jet) produces cavities with a narrow waist for both the stratified and constant-density cloud environments. Model M3 (latitude-dependent wind) only starts to develop a waist in the more time-advanced frame shown in Figure 4 (corresponding to $t = 2800$ yr). In addition, somewhat surprisingly, the straight jet simulations (model M1) show wider cavities than the precessing jet simulations (model M2).

4. CONCLUSIONS

The *Spitzer* observations of HH 46/47 show that the southwest lobe of this outflow has a well-defined, limb-brightened cavity, which joins the source to the (optically visible) condensation 47C. This cavity has its maximum width at $\approx$0.43 of the length of the lobe and a length-to-width ratio of $\approx$3.6. Correcting for the 35° orientation angle between HH 46/47 and the plane of the sky, we then obtain an intrinsic length-to-width ratio $L/D \approx 4.5$. The observed cavity is clearly narrower at the position of the source than farther out along the southwest lobe of the outflow.

Model M1 (straight jet) produces a cavity with $L/D \approx (2.6, 3.0)$, model M2 (precessing jet) a cavity with $L/D \approx (3.1, 4.6)$, and model M3 (latitude-dependent wind) one with $L/D \approx (1.9, 2.7)$ at the time at which the head of the jet emerges from the dense cloud (bottom panels of Figs. 2–4). In the pairs of numbers within parentheses given here, the first number corresponds to the simulations with a constant-density cloud, and the second to the simulations with a stratified cloud. At the more evolved time frames shown in Figures 2–4,

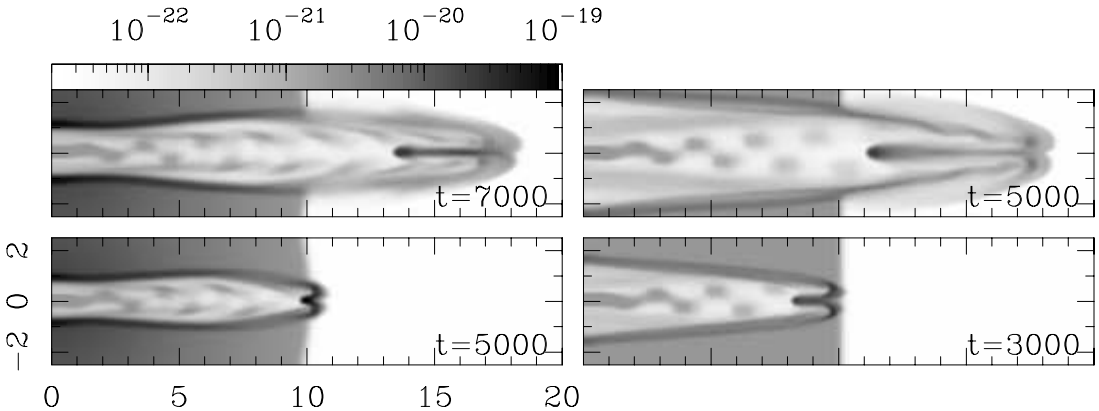

FIG. 3.—Same as Fig. 2, but for model M2 (precessing jet). In this case, the density stratifications shown correspond to the x-z plane, which includes the axis around which the jet is precessing. The right panels correspond to the constant density cloud environment, and the left panels to the stratified cloud environment.

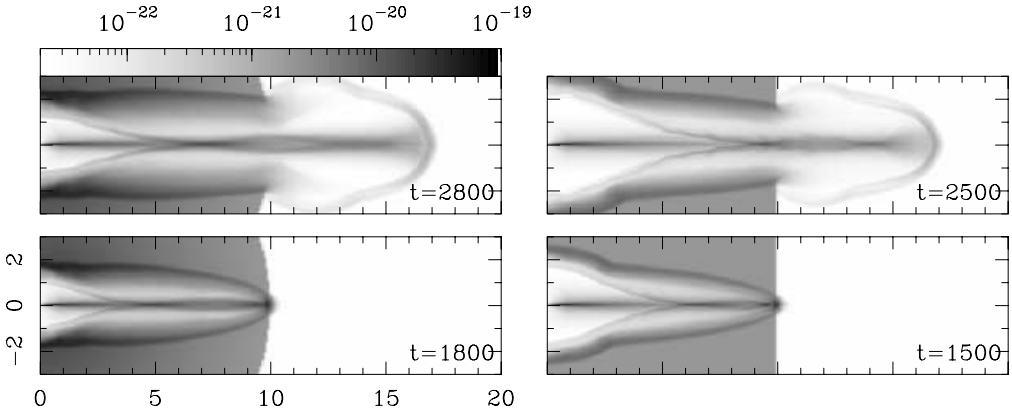

FIG. 4.—Same as Fig. 2, but for model M3 (latitude-dependent wind).

the length-to-width ratios are $L/D \approx (3.5, 3.8)$, (4.1, 5.6), and (2.7, 2.8) for models M1, M2, and M3, respectively (here again the first numbers refer to the constant-density cloud models, and the latter ones to the models with a stratified cloud). Therefore, the model at the time when the jet emerges from the cloud with the length-to-width ratio closest to the value observed for the cavity of the southwest lobe of HH 46/47 is the one with a precessing jet (model M3) moving within a stratified cloud.

As we have said in § 2, it is unclear whether or not knot 47C lies close to the point at which the jet emerges from the dense cloud. If HH 47C were located substantially beyond this point, a comparison of the southwest lobe of HH 46/47 with the more evolved flows in the right panels of Figures 2–4 might actually be more appropriate.

Let us now answer the four questions that were posed in § 1:

With a standard jet (i.e., perfectly collimated, nonprecessing) model, one actually does obtain cavities that resemble the *Spitzer* observations of the southwest lobe of HH 46/47 (see Figs. 1–2).

With the precessing jet model, we actually obtain a cavity that resembles the observations more closely, but it is hard to say whether or not the improvement over the standard jet model is significant.

With the latitude-dependent wind model, we produce cavities that are significantly wider than the one of the southwest lobe of HH 46/47. With other choices of parameters for the latitude-dependent wind (for example, for a wind with the same value of $\theta_0 = 2^\circ$ but with a mass-loss rate of $10^{-7}\ M_\odot\ \mathrm{yr}^{-1}$), we are able to obtain cavities with length-to-width ratios closer to the observed value. Given the fact that the jet models appear to work so well, we conclude that the observed cavity shape cannot be considered as evidence for the presence of a latitude-dependent wind rather than an outflow in the form of a perfectly collimated jet.

For the three outflow configurations that we have considered, it is clear that introducing a stratified cloud environment produces a narrower waist for the cavity, in better agreement with the observations.

Given the limited parameter study presented here, it is clear that it will be possible to obtain better models for the IR cavity of the southwest lobe of HH 46/47. In addition, it will be necessary to include the details of the production of the observed IR emission. In order to do this, one will have to wait for new, spectroscopic observations with *Spitzer*, which will indicate which are the relevant processes for modeling the emission.

We should finally point out that many of the features seen in the simulations presented here have been previously noted by other authors. For example, the "necks" of the cavities produced by jets moving in a stratified environment were modeled by Cabrit et al. (1997). Another feature not described above are the axial "stagnation knots" obtained in the precessing jet simulations (see the right panels of Fig. 3) and which have been modeled by Lim (2001) and Steffen et al. (2001). Models of outflows originating from latitude-dependent winds have been presented by Lery et al. (2002). However, given the fact that the present paper is focused only on the production of cavities and not on the details of the dynamics of the resulting flows, it is not possible for us to describe the previous theoretical work with any kind of justice.

The work of A. R., R. G., and P. V. was supported by the CONACyT grants 36572-E and 41320 and the DGAPA (UNAM) grant IN 112602. We thank Israel Díaz and Antonio Ramírez for support with the computer servers in which the numerical simulations were carried out.

REFERENCES

Beltrán, M. T., Gueth, F., Guilloteau, S., & Dutrey, A. 2004, A&A, 416, 631
Cabrit, S., Raga, A. C., & Gueth, F. 1997, in IAU Symp. 182, Herbig-Haro Flows and the Birth of Stars, ed. B. Reipurth & C. Bertout (Dordrecht: Kluwer), 163
Downes, T. P., & Cabrit, S. 2003, A&A, 403, 135
Eislöffel, J., Davis, C. J., Ray, T. P., & Mundt, R. 1994, ApJ, 422, L91
Eislöffel, J., & Mundt, R. 1994, A&A, 284, 530
Fridlund, C. V. M., & Liseau, R. 1998, ApJ, 499, L75
Gueth, F., Guilloteau, S., & Bachiller, R. 1998, A&A, 333, 287
Hartigan, P., Morse, J. A., & Raymond, J. C. 1994, ApJ, 436, 125
Lee, C.-F., Mundy, L. G., Stone, J. M., & Ostriker, E. C. 2002, ApJ, 576, 294
Lery, T., Henriksen, R. N., Fiege, J. D., Ray, T. P., Frank, A., & Bacciotti, F. 2002, A&A, 387, 187
Li, Z. Y., & Shu, F. H. 1996, ApJ, 468, 261
Lim, A. 2001, MNRAS, 327, 507
Meaburn, J., & Dyson, J. E. 1987, MNRAS, 225, 863
Mundt, R., Ray, T. P., & Raga, A. C. 1991, A&A, 252, 740
Noriega-Crespo, A., et al. 2004, ApJS, 154, 352
Raga, A. C., de Gouveia Dal Pino, E. M., Noriega-Crespo, A., Mininni, P. D., & Velázquez, P. F. 2002, A&A, 392, 267

Raga, A. C., Navarro-González, R., & Villagrán-Muniz, M. 2000, Rev. Mex. AA, 36, 67
Raymond, J. C., Morse, J. A., Hartigan, P., Curiel, S., & Heathcote, S. 1994, ApJ, 434, 232
Reipurth, B., Bally, J., Graham, J. A., Lane, A. P., & Zealy, W. J. 1986, A&A, 164, 51
Reipurth, B., & Heathcote, S. 1991, A&A, 246, 511
Reipurth, B., Yu, K. C., Heathcote, S., Bally, J., & Rodríguez, L. F. 2000, AJ, 120, 1449
Richer, J. S., Hills, R. E., & Padman, R. 1992, MNRAS, 254, 525
Rodríguez, L. F., Cantó, J., Moreno, M. A., & López, J. A. 1989, Rev. Mex. AA, 17, 111
Rodríguez, L. F., Porras, A., Claussen, M. J., Curiel, S., Wilner, D. J., & Ho, P. T. P. 2003, ApJ, 586, L137
Rosen, A., & Smith, M. D. 2004, A&A, 413, 593
Schwartz, R. D. 1977, ApJ, 212, L25
Shu, F. H., Najita, J., Ostriker, E. C., & Shang, H. 1995, ApJ, 455, L155
Steffen, W., López, J. A., & Lim, A. 2001, ApJ, 556, 823
Stocke, J. T., Hartigan, P. M., Strom, S. E., Strom, K. M., Anderson, E. R., Hartmann, L. W., & Kenyon, S. J. 1988, ApJS, 68, 229

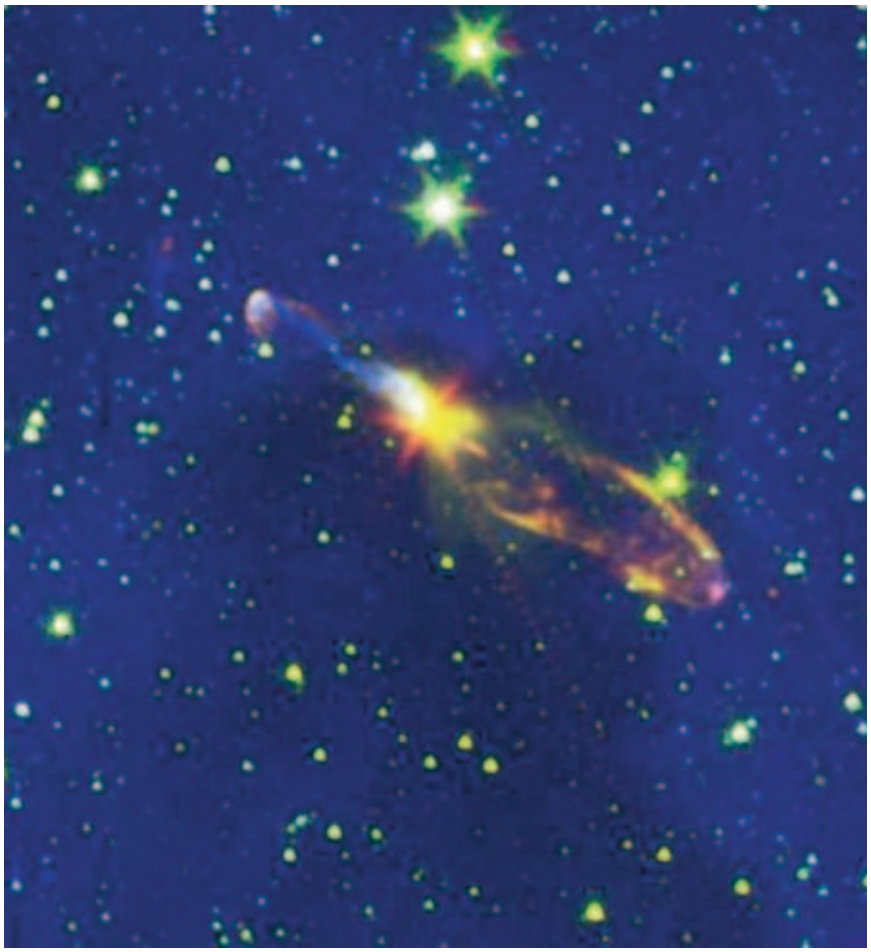

FIG. 1.—*Spitzer* image of the HH 46/47 outflow, which combines the maps in the IRAC bands 1 (3.6 μm, *green*) and 2 (4.5 μm, *red*) superposed on a [S II] 6710+30 image of the same region (*blue*). The knot in the top left corner is HH 47A, and the knot in the bottom right corner is HH 47C. The map shows a region of $5'' \times 6''$. North is up, and east is to the left.